THE JOURNAL OF BIOLOGICAL CHEMISTRY VOL. 292, NO. 8, pp. 3074–3088, February 24, 2017

Sphingosine and Sphingosine Kinase 1 Involvement in Endocytic Membrane Trafficking*

Received for publication, October 7, 2016, and in revised form, December 22, 2016 Published, JBC Papers in Press, January 3, 2017, DOI 10.1074/jbc.M116.762377

Santiago Lima,[1] **Sheldon Milstien, and Sarah Spiegel**[2]

From the Department of Biochemistry and Molecular Biology and Massey Cancer Center, Virginia Commonwealth University School of Medicine, Richmond, Virginia 23298

Edited by Thomas Söllner

The balance between cholesterol and sphingolipids within the plasma membrane has long been implicated in endocytic membrane trafficking. However, in contrast to cholesterol functions, little is still known about the roles of sphingolipids and their metabolites. Perturbing the cholesterol/sphingomyelin balance was shown to induce narrow tubular plasma membrane invaginations enriched with sphingosine kinase 1 (SphK1), the enzyme that converts the bioactive sphingolipid metabolite sphingosine to sphingosine-1-phosphate, and suggested a role for sphingosine phosphorylation in endocytic membrane trafficking. Here we show that sphingosine and sphingosine-like SphK1 inhibitors induced rapid and massive formation of vesicles in diverse cell types that accumulated as dilated late endosomes. However, much smaller vesicles were formed in SphK1-deficient cells. Moreover, inhibition or deletion of SphK1 prolonged the lifetime of sphingosine-induced vesicles. Perturbing the plasma membrane cholesterol/sphingomyelin balance abrogated vesicle formation. This massive endosomal influx was accompanied by dramatic recruitment of the intracellular SphK1 and Bin/Amphiphysin/Rvs domain-containing proteins endophilin-A2 and endophilin-B1 to enlarged endosomes and formation of highly dynamic filamentous networks containing endophilin-B1 and SphK1. Together, our results highlight the importance of sphingosine and its conversion to sphingosine-1-phosphate by SphK1 in endocytic membrane trafficking.

Internalization of extracellular cargo and plasma membrane proteins by endocytic pathways governs many aspects of cell homeostasis and is inextricably linked with cellular signaling, plasma membrane recycling, pathogen entry, and nutrient uptake (1). Much has been learned about how the extensive network of transporting vesicles between membranous organelles is orchestrated by the coordination of endocytic factors and their interactions with membrane lipids (2, 3). Although the balance between cholesterol and sphingolipids within the plasma membrane has long been implicated in endocytic membrane trafficking (4, 5), in contrast to cholesterol functions, little is still known about the roles of sphingolipids. However, genetic studies in yeast have suggested a functional link between sphingolipid metabolism and the endophilin homologs RVS161 and RVS167, which are Bin/Amphiphysin/Rvs (N-BAR)[3] domain-containing endocytic proteins (6, 7). Endophilins recruit dynamin and deform membranes and thus have essential roles in membrane curvature sensing and remodeling (8). Mutation of several genes in sphingolipid biosynthesis can also suppress endocytic defects resulting from deletion of RVS genes (6), and aberrant regulation of membrane sphingolipids interfered with their functions (7). A plasma membrane quantitative genetic interaction map further validated the links of eisosomes, protein-based structures that generate invaginations at the plasma membrane, with sphingolipid metabolism and endosomal trafficking (9).

Sphingosine kinases (SphKs), key enzymes that regulate the levels of the bioactive interconvertible sphingolipid metabolites sphingosine and sphingosine-1-phosphate (S1P), modulate endolysosomal trafficking of the *Drosophila* G protein-coupled receptor rhodopsin (10). Further, local conversion of sphingosine to S1P by SphK1 at presynaptic terminals was shown to be involved in synaptic vesicle recycling and neurotransmitter release in *Caenorhabditis elegans* (11, 12). Previous studies have also shown that SphK1 is localized to early endosomes in COS7 cells (13) and recruited to nascent phagosomes in human macrophages (14). Moreover, the localization and activity of SphK1 were coordinately regulated with actin dynamics during macrophage activation (15).

* This work was supported by National Institutes of Health Grants (K22 CA187314 (to S. L.) and R01GM043880 (to S. S.). The VCU Lipidomics and Microscopy Cores are supported in part by funding from the National Institutes of Health, NCI Cancer Center Support Grant P30 CA016059. The authors declare that they have no conflicts of interest with the contents of this article. The content is solely the responsibility of the authors and does not necessarily represent the official views of the National Institutes of Health.

[1] To whom correspondence may be addressed: Dept. of Biochemistry and Molecular Biology, Virginia Commonwealth University School of Medicine, 1101 E. Marshall St., Richmond, VA 23892. Tel.: 804-828-9330; E-mail: santiago.lima@vcuhealth.org.

[2] To whom correspondence may be addressed: Dept. of Biochemistry and Molecular Biology, Virginia Commonwealth University School of Medicine, 1101 E. Marshall St., Richmond, VA 23892. Tel.: 804-828-9330; E-mail: sarah.spiegel@vcuhealth.org.

[3] The abbreviations used are: N-BAR, Bin/Amphiphysin/Rvs; SphK, sphingosine kinase; S1P, sphingosine-1-phosphate; MEF, mouse embryonic fibroblast; NBD-cholesterol, 25-[*N*-[(7-nitro-2–1,3-benzoxadiazol-4-yl) methyl]amino]-27-norcholesterol; NBD-sphingosine, ω(7-nitro-2–1,3-benzoxadiazol-4-yl)(2S,3R,4E)-2-aminooctadec-4-ene-1,3-diol; MβCD, methyl-β-cyclodextrin; CTB, cholera toxin β subunit; UVRAG, UV radiation resistance-associated gene protein; PF543, 1-[[4-[[3-methyl-5-[(phenylsulfonyl)methyl]phenoxy]methyl]phenyl]methyl]-2R-pyrrolidinemethanol; Sph, sphingosine; RFP, red fluorescent protein; GFP, green fluorescent protein; LC-ESI-MS/MS, liquid chromatography, electrospray ionization, tandem mass spectrometry.

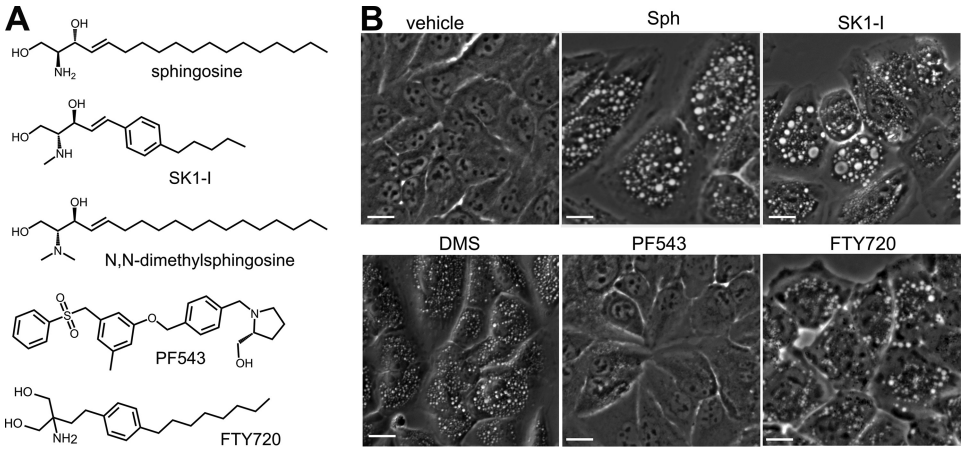

FIGURE 1. **Sphingosine and analogs induce dilated vesicle formation.** *A*, molecular structures of D-*erythro*-sphingosine and the SphK1 inhibitors SK1-I, *N*,*N*-dimethylsphingosine (*DMS*), PF543, and FTY720. *B*, phase-contrast images of H460 cells treated for 30 min with vehicle, sphingosine (10 μM), SK1-I (10 μM), PF543 (1 μM), or FTY720 (5 μM). *Scale bars* = 10 μm.

It has been reported that perturbing the cholesterol/sphingomyelin balance results in massive narrow tubular plasma membrane invaginations enriched with SphK1 through a direct, curvature-sensitive interaction, and it was suggested that accumulation of its substrate, sphingosine, may facilitate SphK1 recruitment (16). SphK1 was also enriched on endocytic intermediates, and down-regulation of SphKs impaired endocytic recycling, suggesting a role for SphK1 and sphingosine phosphorylation in endocytic membrane trafficking beyond the established functions of S1P as a ligand for S1P receptors (16). Because tools needed to determine local changes in SphK1 activity and sphingolipid metabolites in endocytic trafficking are lacking, we resorted to perturbing the balance of sphingolipid metabolites and inhibiting SphK1 activity. We found that treating cells with sphingosine or sphingosine-like lipids induces massive endocytosis, leading to formation of dilated intracellular vesicles that have characteristics of late endosomes, and inhibiting SphK1 activity led to their accumulation. This also led to dramatic changes in the subcellular localization of SphK1 and endophilins A2 and B1. Furthermore, we demonstrated that maintaining the cholesterol/sphingomyelin balance is critical for sphingosine-induced endosomes.

Results

Sphingosine and Its Analogs Induce Formation of Dilated Intracellular Vesicles—Previous studies demonstrated that SphK1 is recruited to tubular endocytic invaginations and suggested that its enzymatic activity is important for endocytic membrane trafficking and recycling (16). To examine the role of the SphK1 substrate sphingosine and its phosphorylation to S1P, H460 non-small cell lung cancer cells were treated with sphingosine (Fig. 1*A*) or SK1-I (Fig. 1*A*), a sphingosine analog that is an isoenzyme-specific SphK1 inhibitor (17). Surprisingly, both produced rapid and extensive formation of dilated intracellular vesicles (Fig. 1*B*). Another sphingosine analog that inhibits SphKs, *N*,*N*-dimethylsphingosine (Fig. 1*A*), also induced dilated vesicles in these cells (Fig. 1*B*). Based on these results, we considered the possibility that inhibiting SphK1 might be sufficient for the formation of vesicles. However, when H460 cells were treated with the non-sphingosine-like but potent SphK1 inhibitor PF543 (18) (Fig. 1*A*), no vesicles were observed, even after extended periods (Fig. 1*B*). In contrast, FTY720, an orally available drug for treatment of multiple sclerosis (19) and a sphingosine analog that inhibits SphK1 (20), also induced dilated intracellular vesicles (Fig. 1*B*) at doses that trigger the internalization of glucose and amino acid transporters (21). Thus, these results suggest that the sphingosine backbone, rather than inhibition of SphK1 activity, mediates the formation of dilated intracellular vesicles. Because vesicles were readily visualized in H460 cells, it was of interest to examine this in other cell types. SK1-I treatment also resulted in massive formation of dilated intracellular vesicles in human DLD1 (Fig. 2*A*) and HCT116 (Fig. 2*B*) colon cancer cells, mouse embryonic fibroblasts (MEFS) (Fig. 2*C*), human breast MCF10A epithelial cells (Fig. 2*D*), and HEK293 cells (data not shown).

Effect of SphK1 Deletion on Vesicle Size and Accumulation—As SphK1 is recruited to early endosomes and other endosomal compartment structures (16), we sought to determine whether SphK1 influenced the size or cellular lifetime of vesicles. To this end, we used *Sphk1*-null MEFs and their wild-type counterparts (Fig. 3, *A*–*C*). As expected, no SphK1 activity could be detected in these *Sphk1*-deficient MEFs (Fig. 3*B*), and cellular levels of S1P were decreased, whereas sphingosine and ceramide levels were increased (Fig. 3*C*). Treatment with the sphingosine-based SphK1 inhibitors SK1-I or FTY720 rapidly formed significantly smaller vesicles in *Sphk1*-deficient MEFs compared with wild-type MEFs, even after prolonged incubations (Fig. 3, *D*–*G*), suggesting that vesicle fusion and enlargement depend on the presence of SphK1.

Although vesicles appeared within 30 min after treatment with SK1-I or with sphingosine (Fig. 1*B*), major differences were obvious after longer incubations (Fig. 4). After 3 h, vesicles in cells treated with sphingosine alone had mostly disappeared (Fig. 4*A*), whereas many were still present in cells treated with SK1-I alone (Fig. 4*A*) and persisted for at least 20 h post-treatment (Fig. 4*B*). In contrast to SK1-I, exogenous sphingosine can be rapidly metabolized not only to S1P but also to ceramide and, subsequently, to complex sphingolipids. Therefore, we next examined the effects of inhibition of SphK1 on the lifetime of

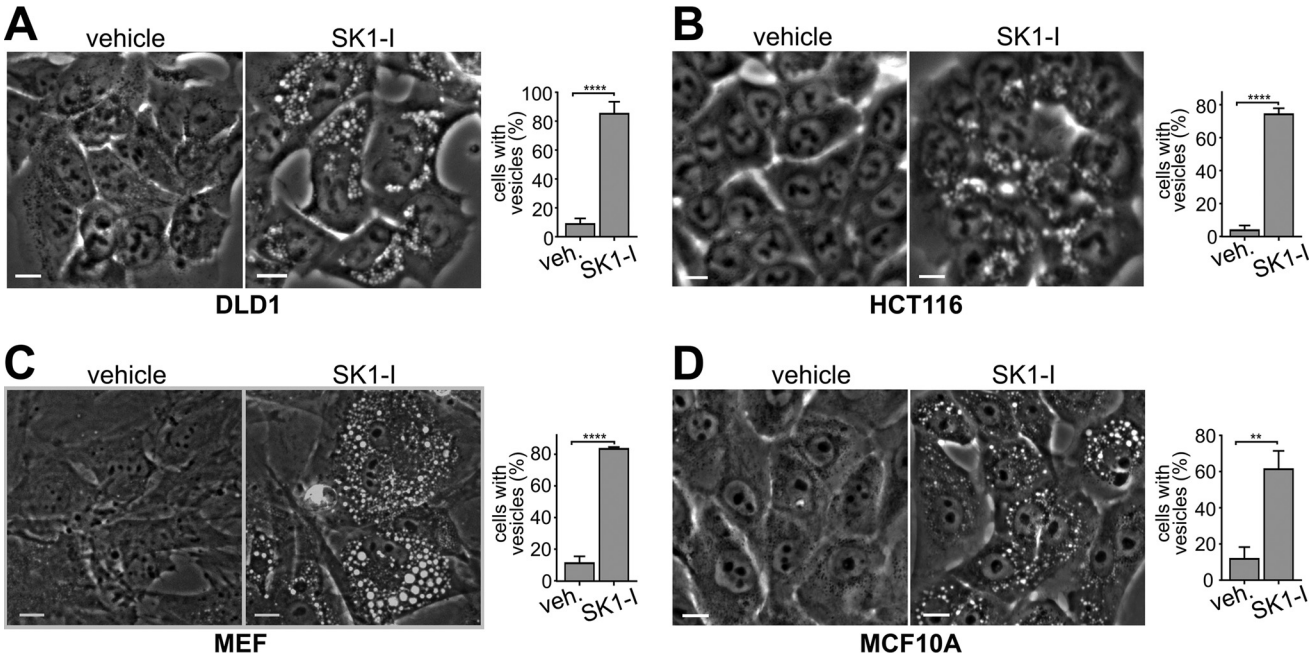

FIGURE 2. **SK1-I, a sphingosine-like SphK1 inhibitor, induces vesicles in diverse cell types.** *A–D*, phase-contrast images and quantification of vesicle-positive cells following 30-min treatment with vehicle (*veh*) or SK1-I (10 μM). *A*, DLD1 colon cancer cells. *B*, HCT116 colon cancer cells. *C*, MEFs. *D*, human breast epithelial MCF10A breast cells. Data are mean ± S.D. **, $p \leq 0.01$; ****, $p \leq 0.0001$. *Scale bars* = 10 μm.

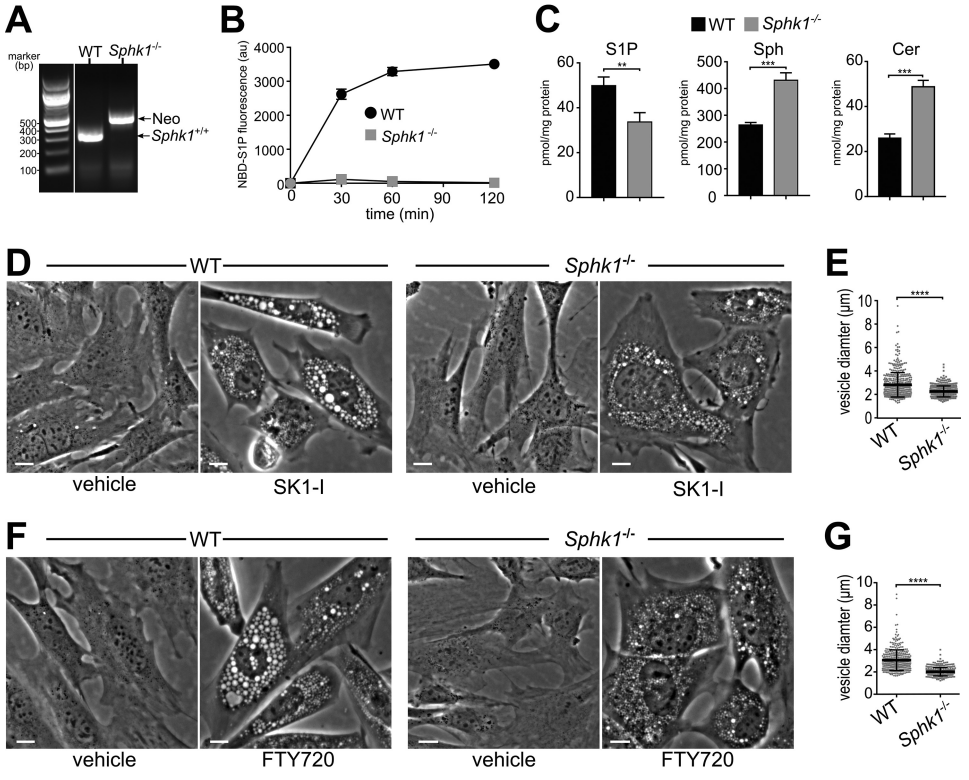

FIGURE 3. **Vesicle size is dependent on SphK1.** *A–C*, characterization of Sphk1 knockout MEFs. *A*, PCR genotyping of wild-type and *Sphk1*$^{-/-}$ MEFs. The expected PCR product for WT *Sphk1* allele amplification is 291 bp and 503 bp for the *Sphk1* knockout neomycin cassette PCR product. *B*, *Sphk1*$^{-/-}$ MEFs showed no activity in a SphK1 isoform-specific activity assay (76). $n = 3$. *C*, sphingolipids were extracted from wild-type and *Sphk1*$^{-/-}$ MEFs, and levels of S1P, Sph, and ceramide (*Cer*) were determined by LC-ESI-MS/MS. Data are mean ± S.D. *D–G*, phase-contrast images (*D* and *F*) and vesicle diameter quantitation (*E* and *G*) of *Sphk1*$^{-/-}$ and WT MEFs treated with vehicle, 10 μM SK1-I for 2.5 h (*D* and *E*), or 5 μM FTY720 for 6 h (*F* and *G*). Data are mean ± S.D. **, $p < 0.01$; ***, $p < 0.001$; ****, $p \leq 0.0001$. *Scale bars* = 10 μm; *au*, arbitrary units.

sphingosine-induced vesicles. When cells were pretreated with the SphK1 inhibitor PF543 followed by prolonged incubation with sphingosine, many dilated vesicles were still present but absent in cells not treated with PF543 (Fig. 4, *A* and *B*). Likewise, deletion of SphK1 also significantly prolonged the lifetime of sphingosine-induced vesicles (Fig. 4, *C* and *D*). Taken together,

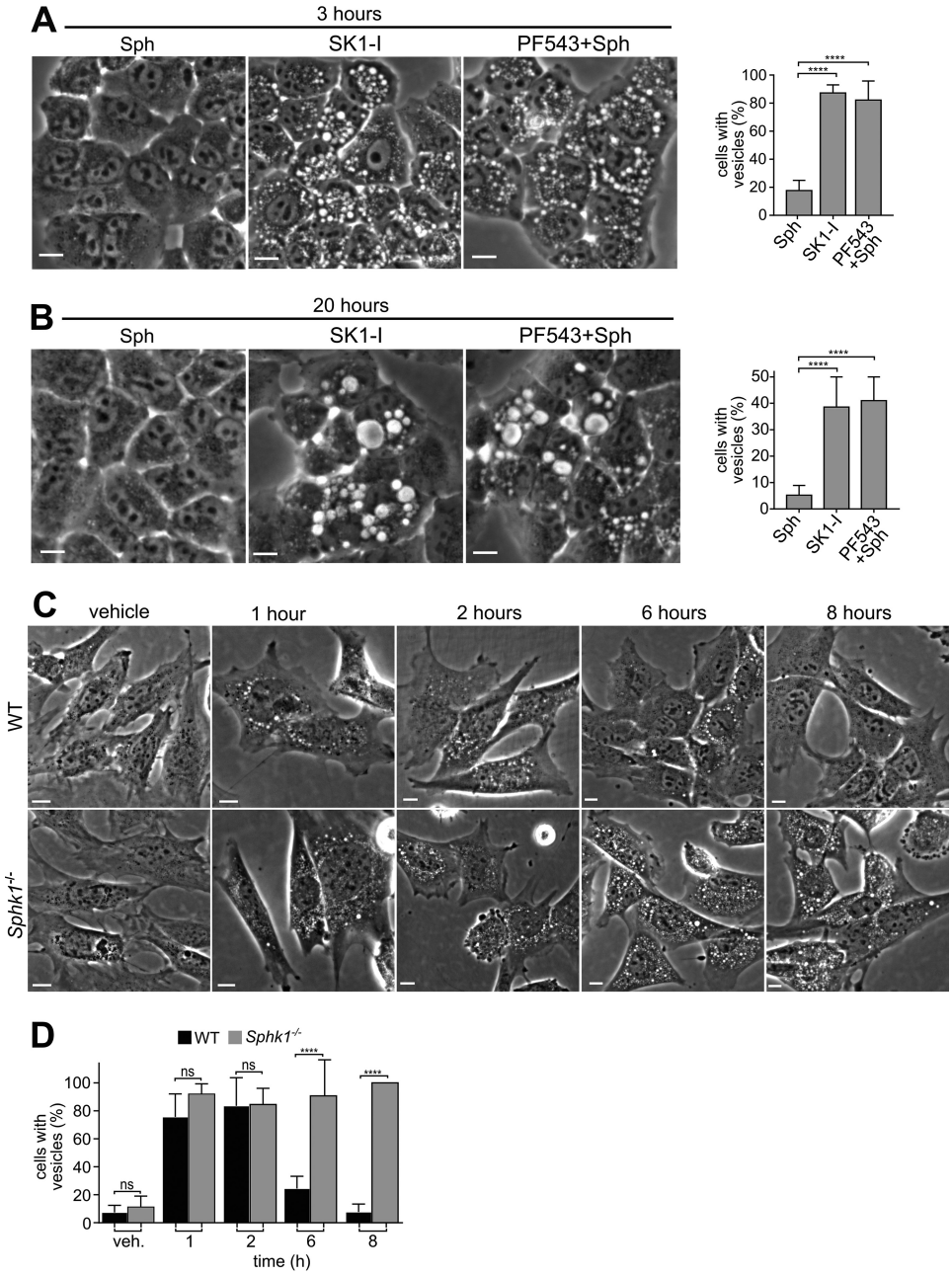

FIGURE 4. **Inhibition of SphK1 leads to accumulation of dilated vesicles.** *A* and *B*, phase-contrast images and quantification of vesicle-positive H460 cells treated with Sph (10 μM) or pretreated with PF543 (1 μM) for 30 min, followed by Sph (10 μM) or SK1-I alone (10 μM) for 3 or 20 h, as indicated. *C* and *D*, wild-type and *Sphk1*$^{-/-}$ MEFs were treated with 10 μM Sph for the indicated times, and vesicle-positive cells were quantified (*D*). At least 5 fields/time point were analyzed. Representative phase-contrast images are shown, and vesicle-positive cells were quantitated. Data are mean ± S.D. *ns*, not significant; ***, $p \leq 0.001$; ****, $p \leq 0.0001$. *Scale bars* = 10 μm. *veh*, vehicle.

these results suggest that the sphingosine backbone is sufficient to induce formation of dilated vesicular bodies and that conversion of sphingosine to S1P by SphK1 is important for their clearance.

Vesicles Are Dilated Late Endosomes—Several approaches were used to examine the subcellular origin of these vesicles. First, prior to addition of SK1-I or sphingosine, cells were pretreated with pHrodo-Red Dextran 10K, which has little to no fluorescence unless it is internalized into acidifiable subcellular compartments such as endosomes (22). Vesicles induced by SK1-I or sphingosine were positive for pHrodo-Red fluorescence (Fig. 5, *A* and *B*) and were clearly much larger than those stained in cells treated with vehicle (Fig. 5*A*). As dextrans of 10K molecular weight are internalized by clathrin-dependent micropinocytosis and macropinocytosis (22), these results suggest that vesicles resulting from treatment with sphingosine or SK1-I originate from the plasma membrane.

It has been suggested that sphingosine acts as a lysosmotropic agent that can affect the integrity of the lysosomal membrane and cause permeabilization in a detergent-like fashion (23). Hence, utilizing acridine orange, a fluorescent weak base that accumulates in acidic organelles, we examined the possibility that SK1-I, which is a sphingosine-like analog, might also have lysosomotropic actions. Chloroquine is a lysosomotropic

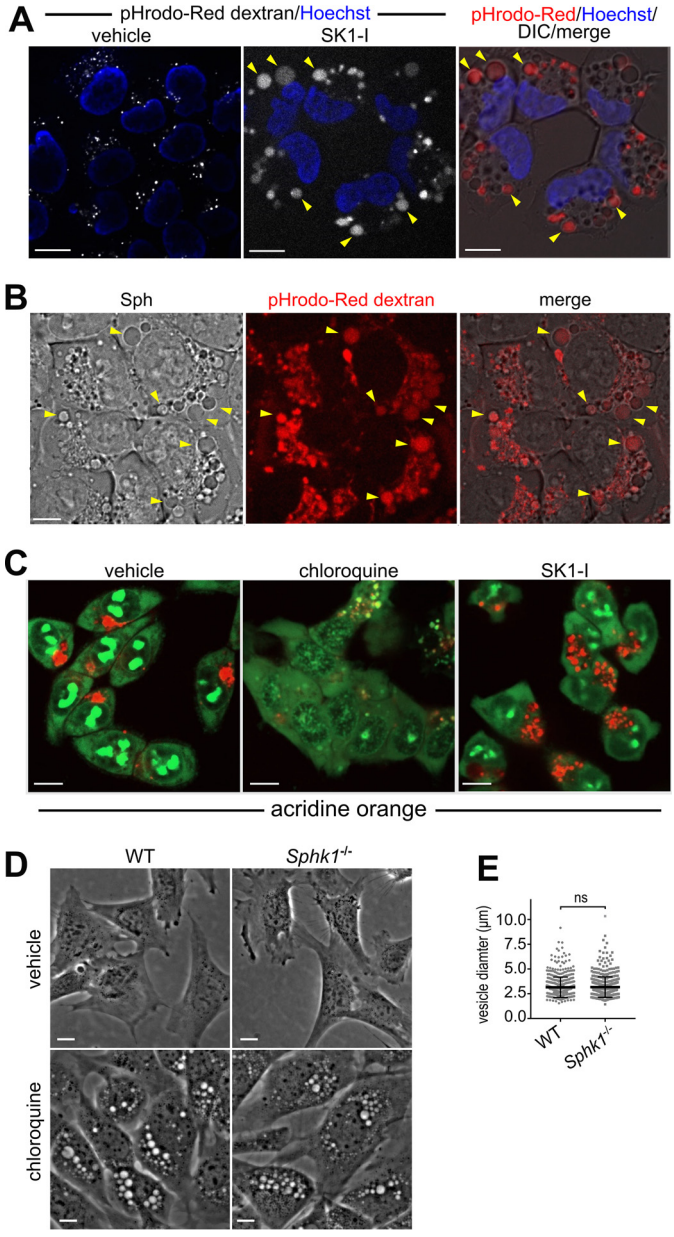

FIGURE 5. **Sphingosine- and SK1-I-induced vesicles are derived from the plasma membrane.** *A* and *B*, phase-contrast and confocal images of live H460 cells pulsed for 15 min with pHrodo-Red-Dextran (0.1 mg/ml) followed by treatment with vehicle, SK1-I (10 μM), or Sph (10 μM) for 30 min as indicated. *Arrowheads* indicate pHrodo-Red-positive dilated vesicles. Nuclei were labeled with Hoechst. *C*, confocal images of live HCT116 cells treated for 5 h with vehicle, chloroquine (50 μM), or SK1-I (10 μM), followed by staining with acridine orange (250 nM). *D* and *E*, phase-contrast images of WT and *Sphk1*$^{-/-}$ MEFs were treated with vehicle or 50 μM chloroquine for 7 h (*D*), and vesicle diameter was quantified (*E*). The data in *E* are mean ± S.D. *ns*, not significant. *Scale bars* = 10 μm.

agent that enters acidic organelles and acts as a strong pH quencher that causes lysosomal swelling (24, 25). As expected, chloroquine severely abrogated acidic organelle staining with acridine orange (Fig. 5*C*). In stark contrast, SK1-I had little to no effect on acridine orange acidic staining compared with vehicle controls (Fig. 5*C*), suggesting that it is unlikely that formation of dilated vesicles induced by SK1-I are engorged acidic organelles. Noteworthy, in contrast to sphingosine-based SphK1 inhibitors that induce much smaller vesicles in *Sphk1*$^{-/-}$ MEFs (Fig. 3), the size of the chloroquine-induced vesicles was similar in *Sphk1*$^{-/-}$ and wild-type MEFs (Fig. 5*D*), suggesting that chloroquine induces vesicle accumulation by a process that is independent of SphK1.

Cholesterol is an important molecular component of the plasma membrane and is involved in endosomal trafficking (3, 26–28). Hence, vesicle formation with SK1-I was examined after labeling with NBD-cholesterol. Dilated vesicles resulting from SK1-I treatment were clearly positive for NBD-cholesterol (Fig. 6*A*) and were also labeled with NBD-sphingosine (Fig. 6*B*), consistent with the observation that a fluorescent sphingosine analog localized to late endosomal and lysosomal vesicles (29). To explore this further, SK1-I-induced vesicle formation was examined in cells expressing Rab7a, a Ras-related protein that is characteristic of the late endosome compartment (30). Dilated vesicles that formed within 30 min after SK1-I treatment were clearly outlined with Rab7a-RFP (Fig. 6, *B* and *C*) and were also co-labeled with NBD-sphingosine (Fig. 6*B*). Moreover, consistent with the long lifetime of vesicles produced by SK1-I but not by sphingosine (Fig. 4), there were almost no observable Rab7a-RFP-positive dilated vesicles remaining after treatment of cells with sphingosine for 8 h, whereas there were still numerous large Rab7a-positive vesicles present in SK1-I treated cells at this time (Fig. 6*D*), suggesting that the enlarged Rab7a-coated vesicles are stalled late endosomes that accumulate when SphK1 is inhibited.

The endocytic and autophagic pathways intersect when late endosomes fuse with autophagosomes to form amphisomes and, subsequently, with lysosomes to form autolysosomes (31). Because SK1-I-induced vesicles were Rab7a-positive and Rab7a is also present on autophagosomes (32), we used microtubule-associated protein light chain 3 (LC3), which decorates autophagosomes and autolysosomes (32), to distinguish between dilated endosomal or autophagic vesicles. As shown in Fig. 6*E*, early (1 h) dilated vesicles in SK1-I treated cells were not positive for LC3-RFP-GFP, indicating that they are not autophagosomes. We also measured the RFP:GFP fluorescence ratio of LC3-RFP-GFP to monitor whether SK1-I affected autophagic progression from autophagosomes (less acidic) to amphisomes and autolysosomes (more acidic) (33), attenuating GFP but not RFP fluorescence. However, after short treatment with SK1-I for 1 h or less, the RFP:GFP fluorescence ratio of LC3-RFP-GFP was not changed (Fig. 6*F*).

SK1-I Induces Clathrin- and Caveolin-dependent Endocytosis—Clathrin-coated pits and caveolae are two major endocytic structures by which plasma membrane-derived cargo is transported into cells by coordinated formation of plasma membrane invaginations that are primarily mediated by clathrin or caveolin, respectively (2, 3). Therefore, we examined their involvement in the massive endocytic influx that results from SK1-I treatment. In vehicle-treated H460 or HCT116 cells, clathrin staining was strongest at the plasma membrane (Fig. 7, *A* and *B*). However, 30 min after SK1-I treatment, in both cell types there was a dramatic relocalization of clathrin from the plasma membrane into diffuse perinuclear foci (Fig. 7, *A* and *B*). Similarly, SK1-I induced rapid internalization of caveolin-1, the main component of caveolae (Fig. 7, *A* and *B*), and caveolin-1 and clathrin co-localized at ring-like structures that appeared

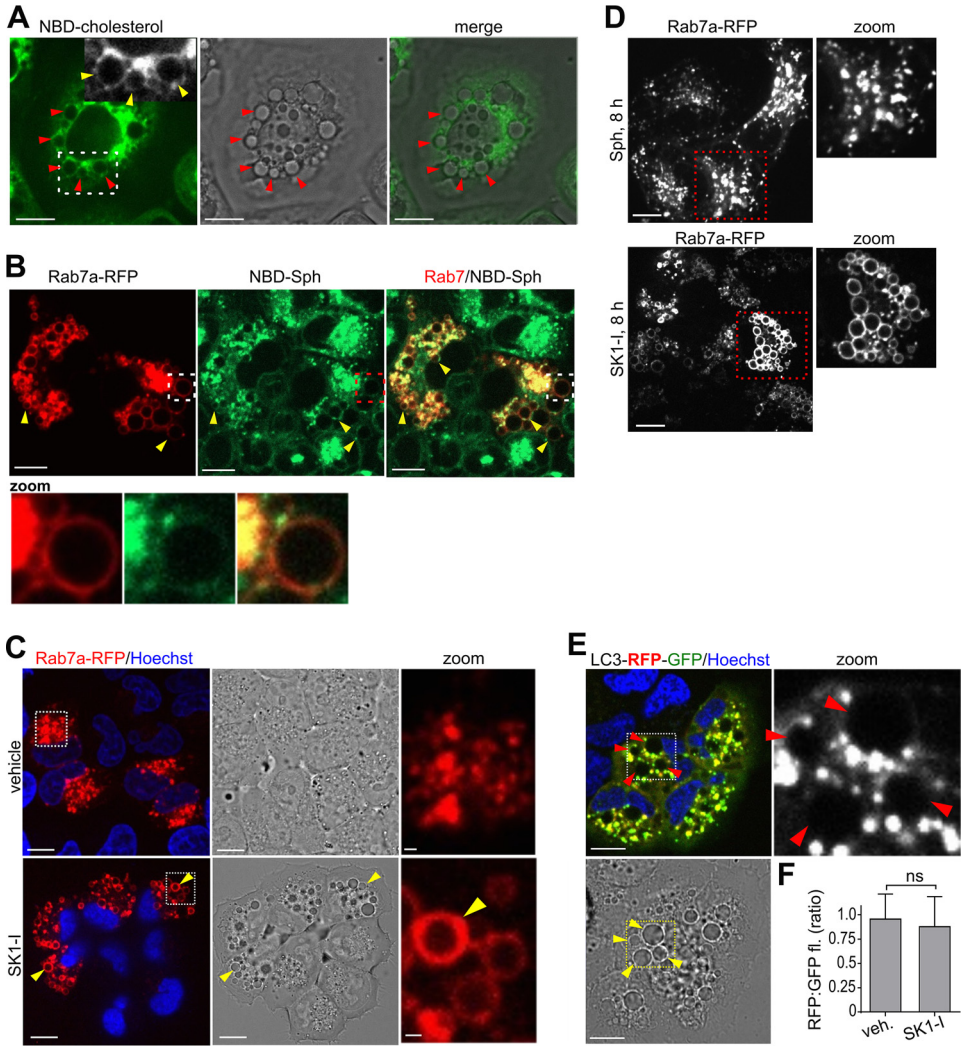

FIGURE 6. **Vesicles are dilated late endosomes.** *A*, phase-contrast and confocal images of live H460 cells pretreated for 20 min with NBD-cholesterol (0.25 μM) followed by SK1-I (10 μM) for 30 min. *Boxed area*, *arrowheads* indicate NBD-cholesterol-positive vesicles. *B*, confocal images of live H460 cells expressing Rab7a-RFP pretreated for 15 min with NBD-Sph (0.25 μM) followed by treatment with SK1-I (7.5 μM) for 30 min. *Zoom*, vesicles positive for NBD-Sph and Rab7a. *C*, confocal and phase-contrast images of live H460 cells expressing Rab7a-RFP treated with vehicle or SK1-I (10 μM) for 30 min. *Zoom*, co-localization of Rab7a to vesicles. *D*, confocal images of live H460 cells expressing Rab7a-RFP treated with Sph (7.5 μM) or SK1-I (7.5 μM) for 8 h. *E* and *F*, confocal and phase-contrast images of H460 cells expressing LC3-RFP-GFP treated with SK1-I (7.5 μM) for 1 h (*E*) and quantification of RFP:GFP fluorescence ratio (*F*). *Zoom*, vesicles were not encircled with LC3-RFP-GFP. *Arrowheads* point to vesicles. In *C* and *E*, nuclei were stained with Hoechst. In *F*, data are mean ± S.D. *ns*, not significant. *Scale bars* = 10 μm.

following treatment (Fig. 7*B*). Live-cell imaging of these cells expressing fluorescently tagged caveolin-1 corroborated these findings (data not shown). To further assess the involvement of caveolin-1, its levels were down-regulated with a specific siRNA. siCaveolin-1 reduced its protein levels by more than 80%, as determined by immunostaining (Fig. 7, *C* and *D*) and immunoblotting (Fig. 7*E*) and significantly reduced vesicle formation in SK1-I treatments, albeit not completely (Fig. 7*F*).

Because down-regulation of clathrin resulted in extensive cell death, we resorted to commonly used inhibitors of endocytosis to examine the involvement of clathrin-dependent and -independent endocytic processes required for SK1-I-mediated endosome formation. Chlorpromazine, a clathrin-dependent endocytosis inhibitor (34, 35), significantly reduced the formation of vesicles induced by SK1-I, whereas nocodazole, a microtubule-disrupting agent, or cytochalasin D1, an inhibitor of actin polymerization, did not have significant effects (Fig. 8, *A* and *B*). On the other hand, bafilomycin A1, an inhibitor of the vacuolar proton pump V-ATPase that disrupts endocytic flow (36), completely blocked SK1-I vesicles (Fig. 8, *A* and *B*). Methyl-β-cyclodextrin (MβCD) has been used extensively to deplete cells of plasma membrane cholesterol, leading to a block in clathrin-dependent (16, 27, 28) and -independent (37) endocytosis. As expected for a plasma membrane-derived endocytic mechanism, cholesterol stripping with MβCD significantly abrogated vesicle formation from SK1-I treatment (Fig. 8, *A* and *B*). A functional link between cholesterol and sphingomyelin, which interact within the plasma membrane (38), and endocytic membrane traffic has been suggested (16). Consistent with this notion, sphingomyelinase, which also disrupts lipid rafts by reducing plasma membrane levels of sphingomyelins (39), blocked SK1-I induced vesicle formation (Fig. 8, *A* and *B*).

Because our results suggest that sphingosine-based SphK1 inhibitors enter the cell via lipid raft-mediated endocytosis, we next utilized cholera toxin β subunit (CTB), which binds on the cell surface to ganglioside GM1, a component of lipid rafts, and

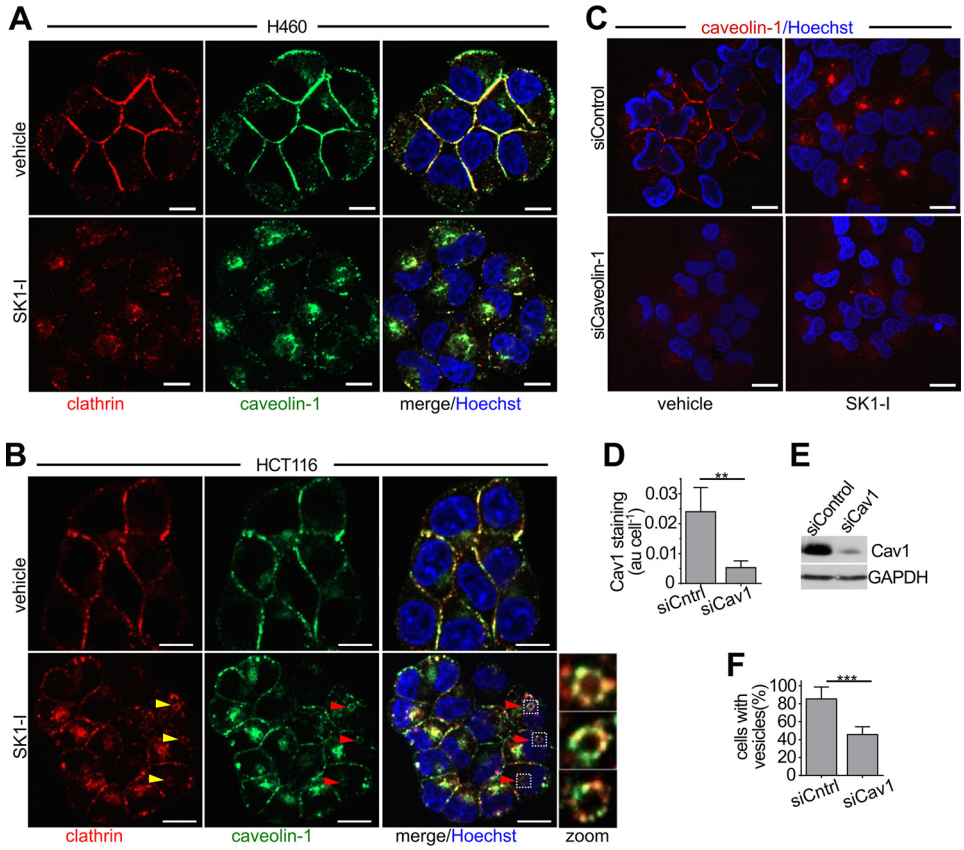

FIGURE 7. **SK1–1 induces internalization of clathrin and caveolin-1.** *A* and *B*, confocal images of H460 (*A*) and HCT116 (*B*) cells treated for 30 min without or with SK1-I (10 μM), followed by immunostaining with anti-clathrin heavy chain (*red*) or anti-caveolin-1 (*green*). *Zoom*, ring-like structures positive for clathrin and caveolin-1 appeared after treatment with SK1-I. *C*, confocal images of H460 cells transfected with non-targeting siControl or caveolin-1 specific siRNA (*siCaveolin-1*). Cells were treated for 30 min with vehicle or SK1-I (10 μM), followed by immunostaining with anti-caveolin-1 (*red*). *D* and *E*, quantification of caveolin-1 fluorescence (*D*) and immunoblots (*E*) of the cells in *C*. $n = 3$. *F*, quantification of vesicle-positive cells in *C*. $n = 5$. In *A–C*, nuclei were stained with Hoechst. Data are mean ± S.D. **, $p \leq 0.01$; ***, $p \leq 0.001$. *Scale bars* = 10 μm; *au*, arbitrary units.

can be internalized through several different endocytic mechanisms, including clathrin-dependent as well as caveolae- and clathrin-independent endocytosis (40, 41). SK1-I significantly increased internalization of CTB in H460 cells (Fig. 8, *C* and *D*), as shown by enhanced intracellular accumulation of fluorescently labeled CTB compared with vehicle-treated controls. In SK1-I treated cells, SK1-I also induced the formation of CTB-positive ring-like structures (Fig. 8*C*). In combination, these results suggest that the sphingosine-like analog SK1-I enters the cell by cholesterol- and sphingomyelin-dependent endocytosis and highlights the importance of the plasma membrane sphingomyelin/cholesterol balance.

SK1-I Induces Recruitment of SphK1 and Endophilins A2 and B1 to Endocytic Intermediates—It was shown previously that perturbing the plasma membrane cholesterol/sphingomyelin balance by cholesterol depletion or treatment with sphingomyelinase results in a delay in the maturation of clathrin-coated pits and rapid formation of clusters of narrow endocytic tubular invaginations containing SphK1 and endophilin-A2 (16), an N-BAR domain-containing protein known to be involved in clathrin-dependent (8) and -independent endocytosis (37, 41, 42). In agreement, within minutes of cholesterol stripping with MβCD, endophilin-A2-GFP relocalized from diffuse puncta into clusters of multiple larger foci (Fig. 9*A*). Likewise, SphK1-GFP, which is mainly cytosolic, was also recruited to foci (Fig. 9*A*), which were similar in kinetics and appearance to those reported previously (16), and V5-tagged SphK1 co-localized with endophilin-A2-GFP at these foci (Fig. 9*B*). We also evaluated the effect of cholesterol stripping on localization of another member of the endophilin family, endophilin-B1, which regulates membrane dynamics of various intracellular compartments involved in endocytosis (8, 43). Unexpectedly, endophilin-B1, which to date has not been clearly demonstrated to be associated with plasma membrane structures (8), was similarly enriched at shallow, delayed-stage clathrin-coated pits following MβCD treatment (Fig. 9*A*). Moreover, V5-tagged SphK1 also co-localized with endophilin-B1-GFP at the foci induced by cholesterol stripping (Fig. 9*C*).

Next, we examined the localization of these proteins following the massive endocytic vesicle formation induced by SK1-I. Unlike acute plasma membrane cholesterol extraction, which resulted in the enrichment of these proteins at shallow plasma membrane endocytic pits (16) (Fig. 9), SK1-I treatment resulted in the recruitment of SphK1-GFP or endophilin-A2-GFP to dilated vesicles (Fig. 10, *A* and *B*, respectively). These results are consistent with previous reports showing that SphK1 is localized on endosomes (13, 16). SK1-I also had a remarkable effect on endophilin-B1, which was intensely enriched at extensive filamentous networks (Fig. 10*C*) that, in some instances, were contiguous with and encircled vesicles (Fig. 10*C*). These fila-

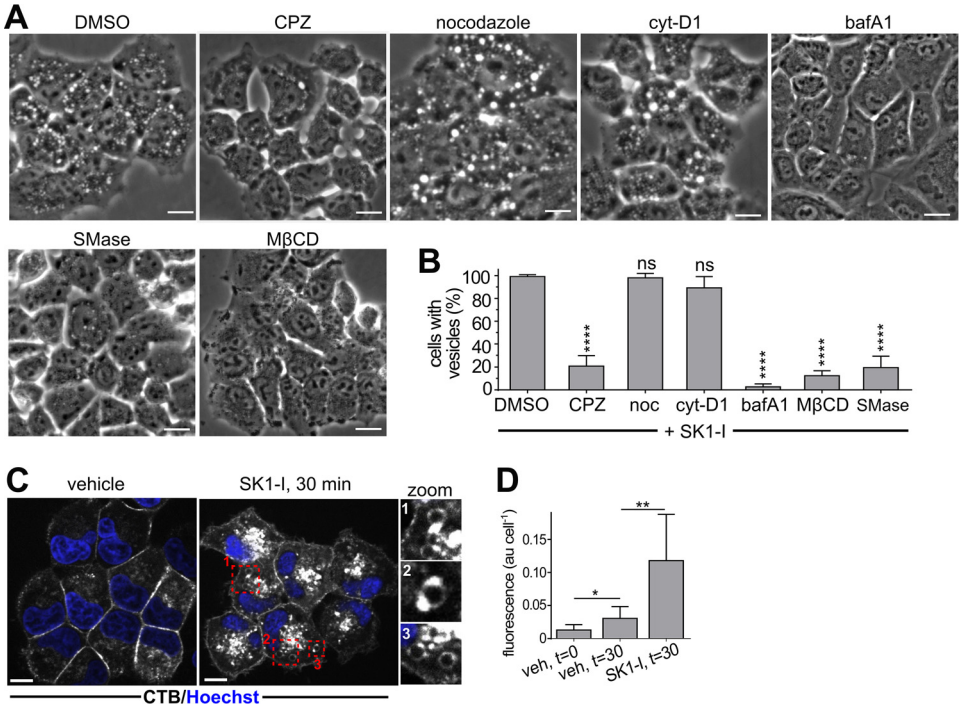

FIGURE 8. **Effect of endocytosis inhibitors.** *A*, phase-contrast images of live H460 cells incubated for 30 min with vehicle (DMSO), chlorpromazine (*CPZ*, 5 μg/ml), nocodazole (*noc*, 200 μM), cytochalasin D1 (*cyt-D1*, 10 μg/ml), bafilomycin A1 (*bafA1*, 50 nM), and MβCD (10 mM) in cholesterol-stripping buffer or acidic sphingomyelinase (*SMase*, 1000 units/ml), followed by treatment with SK1-I (5 μM) for 45 min. *B*, quantification of vesicle-positive cells in *A*. *C* and *D*, SK1-I increases internalization of CTB. Shown are confocal images (*C*) and intracellular CTB fluorescence quantification (*D*) of H460 cells pretreated for 5 min with 0.05 μg/ml Alexa Fluor 647-CTB followed by treatment without or with 10 μM SK1-I for 30 min. *Zoom*, ring-like structures positive for CTB appeared after treatment with SK1-I. At least 80 cells were quantified for each time point. *ns*, not significant; *, $p \leq 0.05$; **, $p \leq 0.01$; ****, $p \leq 0.0001$; *t* test. Data are mean ± S.D. In *C*, nuclei were stained with Hoechst. *Scale bars* = 10 μm. *veh*, vehicle; *au*, arbitrary units.

ments were highly dynamic, having extension and contraction cycles of 2–3 min (Fig. 10*D*, *bottom panels*). Similarly, in some instances, SphK1-GFP assembled as filament-like structures (most likely bundles of tubules) (Fig. 10*E*). In control experiments, GFP alone did not reassemble into filaments and was not recruited to dilated vesicles (data not shown).

The effects of SK1-I on endophilin-B1-GFP and endophilin-A2-GFP localization were not due to an artifact of overexpression because the endogenous proteins showed a similar redistribution. In untreated cells, both endophilins had differential distributions and partially co-localized at hot spots that resembled maturing late-stage clathrin-coated pits (Fig. 11*A*) (16) and had an average diameter of 1.13 μm (Fig. 11*B*). However, upon treatment with SK1-I or PF543 followed by sphingosine, these hot spots reorganized into ring-like structures (Fig. 11, *A* and *C*). These vesicles containing both endophilin-A2 and endophilin-B1 were significantly larger, with an average diameter of 2.73 μm (Fig. 11*B*). SK1-I treatment also induced the formation of elongated filamentous structures that traversed the entire cell volume and were positive for both endophilins (Fig. 11, *A* and *D*). In confocal 3D reconstruction images, filament-like structures positive for endophilin-B1 and endophilin-A2 were clearly present throughout cells treated with SK1-I but not in untreated cells (Fig. 11*D*).

Discussion

Phosphorylation of sphingosine to S1P by SphK1 has been suggested to be involved in endocytic membrane trafficking independent of the canonical actions of S1P as a ligand for S1PR1–5 (16). Because technology with sufficient resolution to examine dynamic changes in endogenous sphingolipid metabolites in cellular membranes during endocytosis has not yet been developed, in this study, using sphingosine or sphingosine-like SphK1 inhibitors to perturb their cellular balance, we sought to gain further understanding of the role SphK1, sphingosine, and S1P play in the regulation of endosomal processes. We have shown that sphingosine-like molecules that enter the cells via lipid rafts induce a massive influx of plasma membrane-derived intracellular endosomes in various cell types. We also established that the sphingosine backbone and not inhibition of SphK1 activity induces the formation of dilated intracellular vesicles. However, further vesicle enlargement depended on the presence of SphK1, as these vesicles were much smaller in *Sphk1*-null MEFs. Our observations that SphK1 is recruited to dilated endosomes and that their clearance is defective when SphK1 is deleted or inhibited indicate that these sphingolipid metabolites and SphK1 are important not only for early steps of endocytosis but also for later stages of endosomal maturation and membrane fusion. FTY720 also enters cells by the same endocytic pathway and induces formation of vesicles whose enlargement is also SphK1-dependent. Because FTY720 is a prodrug that must enter cells to be phosphorylated to its active form (19), understanding its endocytic membrane trafficking may have implications for its clinically relevant actions. While our manuscript was under revision, Wang and co-workers (44) also reported that MEFs treated with SK1-I or sphingosine accumulate enlarged dysfunctional late endosomes. They also showed that SphK1-dependent phosphorylation of sphingosine

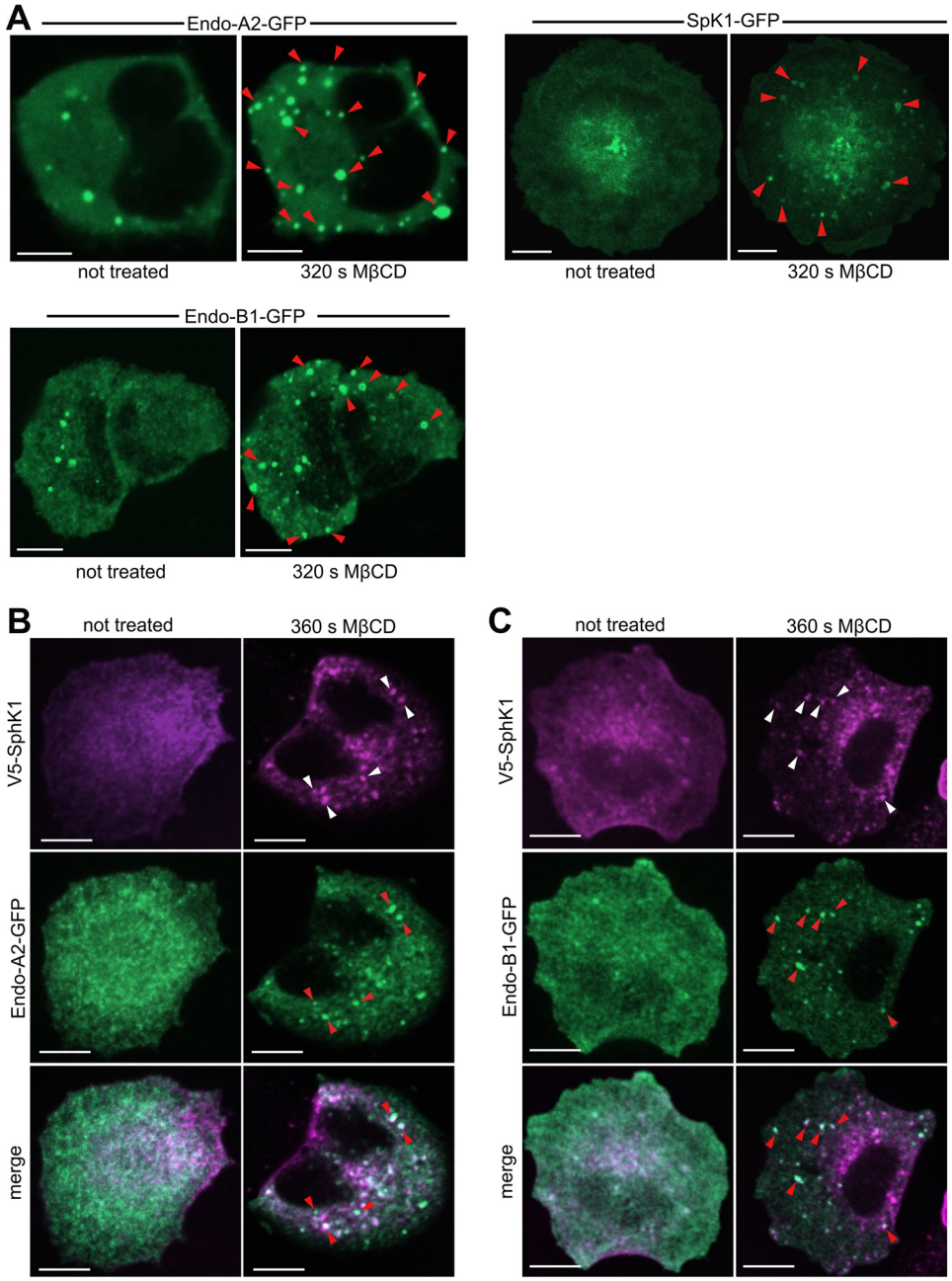

FIGURE 9. **Acute removal of plasma membrane cholesterol induces recruitment of endophilin-A2, endophilin-B1, and SphK1 to tubular invaginations.** *A*, live-cell confocal images of H460 cells expressing endophilin-A2-GFP, SphK1-GFP, or endophilin-B1-GFP, as indicated, before and 320 s after 10 mM MβCD treatment at 37 °C. A total of four independent experiments with a minimum of 5 cells/experiment were performed, and representative images are shown. *B* and *C*, confocal images of H460 cells expressing endophilin-A2-GFP and V5-tagged SphK1 (*B*) or endophilin-B1-GFP and V5-tagged SphK1 (*C*) before and 360 s after 10 mM MβCD treatment at 37 °C and immunostained with anti-V5 (*purple*). *Arrowheads* point to foci formed after MβCD treatment where endophilins and V5-tagged SphK1 co-localize. *Scale bars* = 10 μm.

promoted endocytic membrane trafficking (44). In agreement with our findings, it has been shown that decreased conversion of sphingosine to S1P causes disruption of autophagosome-lysosome fusion (45) and blockade of lysosome recycling (46). Furthermore, elevation of intracellular sphingosine from caged sphingosine induced transient calcium release from lysosomal stores that required the two-pore channel 1 (TPC1) residing on endosomes and lysosomes (29). Deregulation of lysosomal calcium leads to defects in endolysosome fusion (29, 47). Moreover, down-regulation of SphKs results in endocytic recycling defects (16, 48), which could explain the accumulation of enlarged stalled endosomes we observed upon inhibition or deletion of SphK1. Although SphK1 knockout mice do not exhibit any known endocytic phenotype, it should be noted that, although SphK1-deficient mice do not have striking abnormalities (49), SphK1/2 double knockout is embryonic lethal with defective vascularization and highly vacuolated endothelial cells (49). Therefore, it is possible that SphK2 compensates for loss of SphK1 in specific cell types. In agreement with this notion, De Camilli and co-workers (16) have shown that SphK2 was also present at endophilin foci, consistent with redundant functions of SphK1 and SphK2 in mice (49).

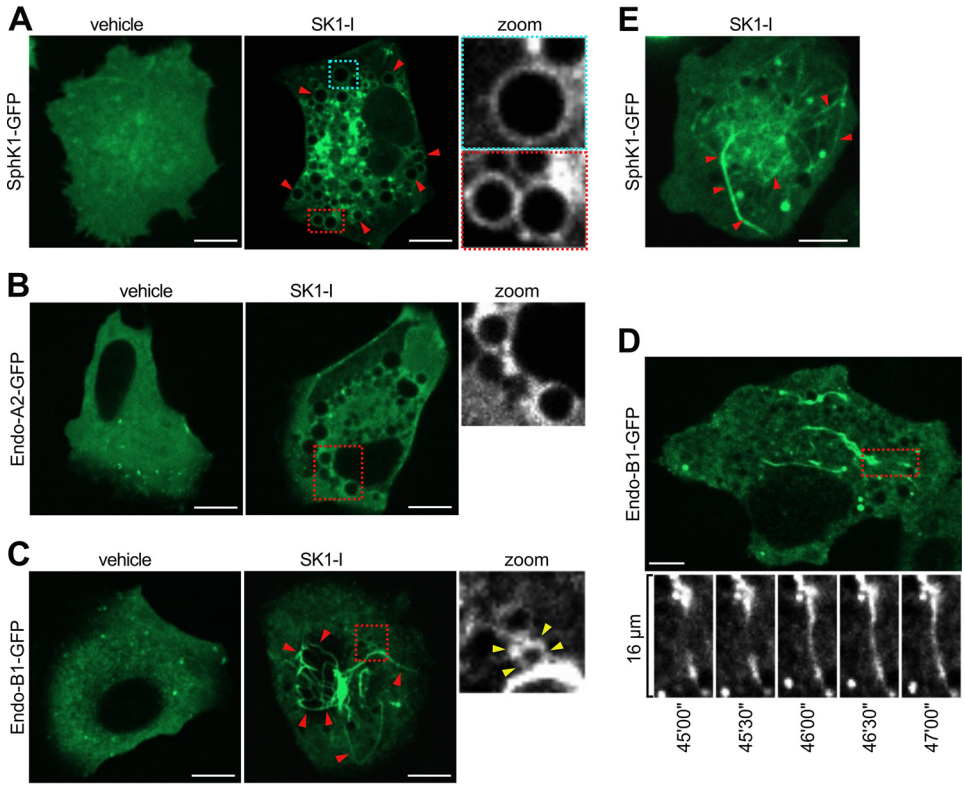

FIGURE 10. **SK1-I induces recruitment of SphK1, endophilin-A2, and endophilin-B1 to vesicles and dynamic filamentous structures.** *A–E*, live-cell confocal images of H460 cells expressing SphK1-GFP (*A* and *E*), endophilin-A2-GFP (*B*), or endophilin-B1-GFP (*C* and *D*) treated with 10 μM SK1-I for 45 min. *D*, *bottom panels*, time-lapse (30-s intervals) images of the region outlined in *red*. *Zoom*, magnification of SphK1-GFP-positive (*A*) or endophilin-A2-GFP-positive (*B*) vesicles and endophilin-B1-GFP positive filaments (*C*). *Arrowheads* in *C* point to filaments that are contiguous with vesicles. *Arrowheads* in *E* point to SphK1-positive filaments. *Scale bars* = 10 μm.

Corroborating previous studies showing that SphK1 is targeted to early endocytic intermediates (16) and that it is highly enriched in nerve terminals involved in synaptic vesicle recycling in *C. elegans* (11, 12), we observed a massive and rapid recruitment of SphK1 to endosomes. Furthermore, it has been suggested that recruitment of SphK1 to membranes involves a direct, curvature-sensitive interaction with the lipid bilayer, possibly by interaction between a hydrophobic patch on its surface and sphingosine (16). In agreement with this, dilated endosomes intensely enriched with SphK1 were also labeled with NBD-sphingosine. In contrast to wild-type SphK1, mutations of SphK1 within this hydrophobic patch did not rescue the neurotransmission defects in *C. elegans* loss-of-function mutants (11, 12).

What is the physiological role of sphingosine-containing endosomes in endocytosis? In yeast, previous studies convincingly demonstrated that long-chain sphingoid bases regulate endocytosis (50, 51). The absence of sphingoid bases led to a defect in the internalization step of endocytosis, which was rescued by 50 μM exogenous sphingoid bases (52) or by overexpression of the kinase Pkc1 (a homolog of PKC) involved in the internalization step of endocytosis (53). Intriguingly, long-chain sphingoid bases activate Pkh1/2 (homologs of PDK1) (54), which, in turn, phosphorylate and activate the downstream kinases Ypk1/2 (homologs of SGK1) and Pkc1, a conserved kinase cascade that controls endocytosis by phosphorylating components of the endocytic machinery (55). Reminiscent of the defect in internalization of α-factor pheromone in yeast with reduced sphingoid bases because of mutations in serine palmitoyltransferase (52), myriocin, an inhibitor of serine palmitoyltransferase, impaired the uptake of transferrin and low-density lipoprotein in mammalian cells (56). It is tempting to speculate that sphingoid bases play an evolutionary conserved role in the internalization step of endocytosis. Although we used indirect genetic and pharmacological approaches to investigate the role of sphingosine and SphK1 in endocytic trafficking, we anticipate that in the future, technology with sufficient resolution to directly follow dynamic changes in endogenous sphingosine and sphingolipid metabolism during membrane trafficking will be developed.

Under physiological conditions, sphingosine is positively charged and has important biophysical properties that influence the behavior of biological membranes (57). Depending on the lipid composition, it can aggregate into gel-like domains with sphingomyelin and cholesterol (58, 59), rigidify membranes (58), and increase the liquid ordered phase fraction in artificial vesicles (59). Because sphingosine acts as a modulator of membrane lipid domains, it was suggested that it can regulate biological responses by direct binding to proteins as well as influence their membrane sorting (59). We speculate that, similar to the effects of lowering plasma membrane cholesterol, changing the levels of sphingosine augments the deformability of the membrane and increases the recruitment of SphK1 and the N-BAR domain-containing proteins endophilin-A2 and endophilin-B1, involved in the sensing and mechanics of membrane curvature (8). We suggest that, in addition to endophi-

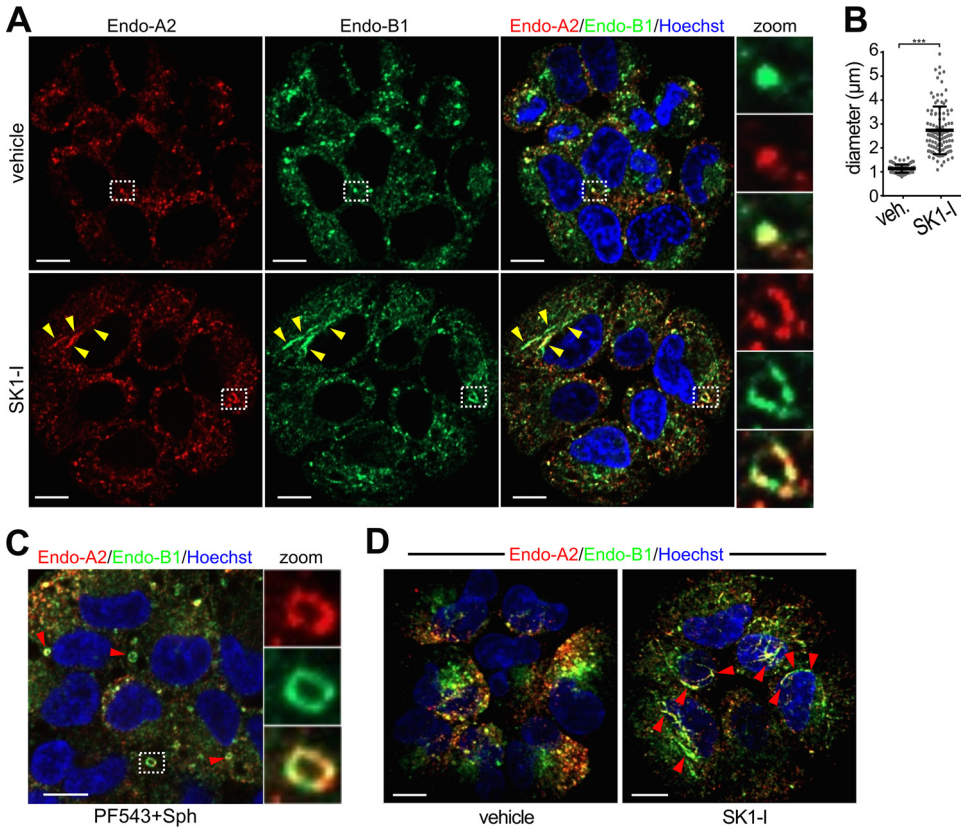

FIGURE 11. **Relocalization of endogenous endophilin-A2 and endophilin-B1 following treatment with SK1-I and sphingosine.** *A*, *C*, and *D*, confocal images of H460 cells treated with vehicle (*A*), 10 μM SK1-I for 30 min (*A* and *D*), or 1 μM PF543 for 30 min followed by 10 μM Sph (*C*) for 30 min. Cells were then immunostained with anti-endophilin-A2 (*red*) or anti-endophilin-B1 (*green*), and nuclei were labeled with Hoechst. *Arrowheads* in *A* point to filamentous structures. *A* and *C*, *zoom*, magnification of double-positive foci (*A*, *top*) and vesicles (*A*, *bottom*, and *C*). *B*, the diameters of foci and vesicles in *A* were determined. *D*, 3D reconstructions of cells treated without or with 10 μM SK1-I for 30 min. A total of 37 0.44-μm slices were collected for each channel. One slice in the *right panel* was used in *A*. Data are mean ± S.D. ***, $p \leq 0.001$. *Scale bars* = 10 μm.

lin-A1 and SphK1, sequestration of endophilin-B1 on tubules may also contribute to the accumulation of shallow clathrin-coated endocytic pits observed previously after changing plasma membrane levels of cholesterol or sphingomyelin (16).

In contrast to the well known function of endophilin-A2 in coordinating the constriction of coated pits in clathrin-mediated endocytosis (8, 60–62), which has recently been broadened to membrane scission and clathrin-independent endocytosis (37, 41), the role of endophilin-B1 in endocytic pathways is not well defined (43). Endophilin-B1 was originally discovered as a Bax-binding protein (63), involved in apoptosis and mitochondrial morphology or fission (43, 64). However, subsequent studies found that it binds to Beclin1 through UV radiation resistance-associated gene protein (UVRAG) to promote activation of class III phosphatidylinositol 3-kinase and autophagosome biogenesis and maturation (43, 65). Nevertheless, our results support an emerging role for endophilin-B1 and SphK1 in intracellular membrane dynamics and endocytosis. Endophilin-B1 interacts directly with and is recruited to the plasma membrane with the exchange factor of the endosomal trafficking regulator Arf6 (66), is associated with early endosomes, and facilitates the delivery of internalized EGF receptors to late endosomes/lysosomes, which suppresses breast cancer cell migration (67). Interaction of UVRAG with the core class C vacuolar protein sorting complex, in addition to promoting autophagosome maturation, is also involved in endosome-lysosome transition by activation of Rab7 (68). It is also possible that binding of endophilin-B1 to UVRAG modulates the interaction with and function of the core class C vacuolar protein sorting complex (69).

Endocytic processes play critical roles in normal cell physiology, and derailed endocytosis has been associated with many human diseases, including cancer, Alzheimer's disease, and lipid storage diseases, to name a few (70–72). Our results further highlight the role of the sphingolipid metabolite sphingosine and SphK1 in the regulation of endocytic membrane trafficking and recruitment of SphK1 and the N-BAR proteins endophilin-A2 and -B1 to endocytic intermediates. Elucidation of the interplay between sphingolipid metabolism and endocytosis will lead to a better understanding of membrane trafficking and dynamics and has the potential to lead to improved therapies for disorders with alterations in the endocytic pathway.

Experimental Procedures

Reagents—SK1-I was from Enzo Life Sciences (catalog no. BML-EI411) and was dissolved in water. D-*erythro*-sphingosine (Avanti Lipids, catalog no. 860490) and NBD-sphingosine (ω(7-nitro-2–1,3-benzoxadiazol-4-yl)(2S,3R,4E)-2-aminooctadec-4-ene-1,3-diol) (Avanti Lipids, catalog no. 810205) were dissolved in ethanol. *N,N*-dimethylsphingosine (Enzo Life Sciences, catalog no. BML-SL105), PF543 (1-[[4-[[3-methyl-5-

[(phenylsulfonyl)methyl]phenoxy]methyl]phenyl]methyl]-2R-pyrrolidinemethanol) (Cayman Chemical, catalog no. 17034), and 25-NBD-cholesterol (25-[*N*-[(7-nitro-2–1,3-benzoxadiazol-4-yl)methyl]amino]-27-norcholesterol) (Avanti Lipids, catalog no. 810250) were dissolved in DMSO. Chlorpromazine hydrochloride, acidic sphingomyelinase, cytochalasin D1, nocodazole, and bafilomycin A1 were from Sigma-Aldrich. Cell culture reagents were from Life Technologies. All other reagents were of chemical grade and were purchased from Sigma-Aldrich or Fisher Scientific.

Cell Culture and Treatments—H460, H1299, DLD1, HEK293T, and MEFs were purchased from the ATCC. *Sphk1*$^{-/-}$ and *Sphk1*$^{+/+}$ MEFs were obtained from H. G. Wang (Penn State University). HCT116 cells were obtained from B. Vogelstein (Johns Hopkins University). All cells were cultured in DMEM containing 10% fetal bovine serum without antibiotics, except for MCF10A cells, which were cultured in DMEM/F12 media containing 5% horse serum, 20 ng/ml EGF, 0.5 mg/ml hydrocortisone, 100 ng/ml cholera toxin, and 10 μg/ml insulin. For live-cell imaging, 50,000 cells/well were seeded in a 24-well glass-bottom dish (Cellvis) and allowed to attach for 48 h. For Western blotting, 350,000 cells/well were seeded in a 6-well dish and allowed to attach for 24 h. For endocytosis inhibitor treatments, cells were incubated for 30 min in media containing 10% serum with either DMSO, chlorpromazine (5 μg/ml), acidic sphingomyelinase (1000 units/ml), nocodazole (200 μM), cytochalasin D1 (10 μg/ml), or bafilomycin A1 (50 nM), followed by addition of SK1-I.

Fluorescent lipids were added to cells on 24-well plates in media containing 10% serum at 37 °C and incubated for 20 min, and then either SK1-I or sphingosine was added directly to cells. Cells incubated with NBD-labeled lipids were imaged by confocal microscopy as described below using 459/529-nm excitation/emission.

Plasmids, siRNA, Transfection, and Overexpression—The endophilin-A2-GFP (catalog no. RG201552) and endophilin-B1-GFP (catalog no. RG200106) plasmids were from Origene, and control scrambled siRNA and siRNA targeting caveolin-1 (catalog no. L-003467) were from Thermo Fisher Scientific. Cells were transfected with siRNAs using Lipofectamine RNAiMAX reagent (Thermo Fisher Scientific) following the guidelines of the supplier. The endophilin-A2-GFP, endophilin-B1-GFP, V5-SphK1 (73), and SphK1-GFP (74) plasmids were transfected with Polyjet (SignaGen Laboratories) as follows: 2.5×10^6 cells were seeded on 10-cm dishes and allowed to attach for 24 h. Plasmid-transfection reagent mixtures were prepared following the guidelines of the manufacturer and incubated with cells for 4 h, transfection media was replaced with fresh media containing 10% serum, and cells were allowed to rest for 1 h. Cells were then trypsinized and seeded at 50,000 cells/well in 24-well glass-bottom plates and allowed to attach for 48 h. The viral particles used for overexpression of Rab7a-RFP (catalog no. C10589) and LC3-RFP-GFP (catalog no. P36239) were obtained from Life Technologies, and cells were infected with 20 μl of viral particles/50,000 cells for 48 h.

Imaging—Phase-contrast images were collected on a Zeiss Axiovert 40 CFl inverted microscope equipped with a ×40 phase-contrast objective and an Axiocam MRm camera. All fluorescence confocal microscopy with live or fixed cells on 24-well glass-bottom plates (Cellvis) was performed on a Zeiss Cell Observer spinning disc confocal microscope with a ×63 water/oil objective equipped with an Axiocam MRm camera and two Photometrics Evolve 512 cooled emCCD cameras. For live-cell confocal microscopy, the growth chamber was maintained at 37 °C with 5% CO_2 saturation.

Acridine Orange Staining—Cells cultured in 24-well glass-bottom plates were treated as described in the figure legends and incubated with 250 nM acridine orange (Thermo Fisher Scientific) for 10 min in media containing 10% serum followed by a wash and then imaged by fluorescence microscopy as described above using 488/509-nm excitation/emission for the alkaline indicator (green) and 475/572-nm excitation/emission for the acidic indicator form (red). Confocal fluorescence images were collected as described above using identical settings across all wells.

Cholesterol Stripping—Cholesterol stripping was performed as described previously (16). For experiments, images of cells in 24-well glass-bottom plates were collected prior to MβCD treatment. 1 ml of prewarmed (37 °C) MβCD stripping solution containing 10 mM HEPES (pH 7.4), 120 mM NaCl, 3 mM KCl, 2 mM $CaCl_2$, 2 mM $MgCl_2$, and 10 mM MβCD (Sigma-Aldrich) was added to each well, and the preimaged cells were followed for 7 min.

CTB Internalization—Cells on 24-well glass-bottom plates were pretreated for 5 min with Alexa Fluor 647-CTB (0.05 mg/ml, Life Technologies, catalog no. C34778) in media containing 10% serum. After 5 min, cells were either washed with PBS and then fixed with formalin for 10 min, followed by two PBS washes, or treated without or with SK1-I and then fixed with formalin and washed with PBS. Cell nuclei were labeled with Hoechst for 5 min. Images were collected as described above using identical settings across all wells. Fluorescence intensity was quantified using ImageJ (75).

Immunofluorescence—Following treatments, cells on 24-well glass-bottom plates were washed twice with PBS, fixed with formalin for 10 min, followed by three PBS washes, and then permeabilized for 2 min (Tris-buffered saline, 0.1% Tween 20). Fixed cells were then incubated for 30 min with the following primary antibodies from Santa Cruz Biotechnologies diluted in PBS: caveolin-1 (1:250, catalog no. sc-894), clathrin (1:250, catalog no. sc-6579), endophilin A2 (1:150, catalog no. sc-10876), and endophilin B1 (1:150, catalog no. sc-393191). The anti-V5 antibody (1:250, catalog no. 46-0705) was from Life Technologies. Cells were then incubated for 30 min with the appropriate Alexa Fluor (Life Technologies) fluorescently labeled secondary antibodies: anti-goat (catalog no. A11057), anti-rabbit (catalog no. A11008), or anti-mouse (catalog no. A11001), all diluted (1:400) in PBS. Nuclei were labeled with Hoechst for 5 min, and cells were imaged by confocal microscopy as described above.

Western Blotting—Following treatments, cells were harvested by washing twice with ice-cold PBS and then scraped in 200 μl of buffer containing 20 mM HEPES (pH 7.4), 250 mM NaCl, 1% Triton X-100, 1 mM DTT, 1 mM EDTA, 20% glycerol, and Halt protease and phosphatase inhibitors (Thermo Fisher Scientific). Cell suspensions were sonicated and centrifuged,

and equal amounts of supernatant proteins were separated by SDS-PAGE. Protein concentrations were determined using the Bio-Rad protein assay. Immunoblotting was performed using the SNAP i.d. 2.0 protein detection system (Millipore) with the following antibodies diluted 1:500 in TBS containing 0.1% Tween 20 and 0.05% blotting-grade milk: GAPDH (1:1500, catalog no. 2118, Cell Signaling Technology) and caveolin-1 (1:1000, catalog no. sc-894, Santa Cruz Biotechnology). Immunopositive bands were visualized by enhanced chemiluminescence using secondary antibodies conjugated with horseradish peroxidase and Super-Signal West Pico or Dura chemiluminescent substrates (Pierce).

SphK1 Activity Assay—Assays were performed as described previously (76). Briefly, *Sphk1*$^{+/+}$ and *Sphk1*$^{-/-}$ MEFs cultured on 10-cm dishes were washed twice with ice-cold PBS, harvested in buffer (400 μl/10-cm dish) containing 30 mM Tris (pH 7.4), 150 mM NaCl, 10% glycerol, and 0.2% Triton X-100 and supplemented with Halt protease and phosphatase inhibitors (Thermo Fisher Scientific). Cell suspensions were sonicated and extracts clarified by centrifugation. Assays contained equal amounts of cell extracts and 50 μM NBD-sphingosine (Avanti Lipids) and were adjusted to 0.25% Triton X-100. Reactions were initiated with 20× Mg-ATP mixture (20 mM ATP, 200 mM $MgCl_2$, 800 mM Tris (pH 7.4) and incubated at 37 °C. At each time point, an equal volume of 1 M KPO_4 (pH 8.5) and 5 volumes of 2:1 chloroform:methanol were added, followed by vigorous vortexing and 5-min centrifugation. A portion of the upper aqueous layer was read at 463/536-nm excitation/emission wavelengths on a fluorescence microplate reader.

Statistical Analysis—All experiments were repeated independently a minimum of three times with consistent results, and representative data are shown. Statistical analyses were performed using unpaired two-tailed Student's *t* test for comparison of two groups and analysis of variance followed by post hoc tests for multiple comparisons (GraphPad Prism). For all analyses, $p \leq 0.05$ was considered statistically significant.

Author Contributions—S. L. performed all experiments, analyzed the data, and wrote the paper with assistance from S. M. and S. S. S. S. conceived and coordinated the study. All authors reviewed the results and approved the final version of the manuscript.

Acknowledgments—We thank Dr. Michael Maceyka and Dr. Jason Newton for valuable insights and discussions, Dr. Scott Henderson for assistance with all microscopy-related topics, Dr. Jeremy Allegood for skillful sphingolipid analyses, and Dr. Timothy Rohrbach and Melissa Maczis for assistance with MEF cell genotyping. We thank H. G. Wang (Penn State University) for kindly providing us with wild-type and Sphk1$^{-/-}$ *MEFs.*

References

1. Sigismund, S., Confalonieri, S., Ciliberto, A., Polo, S., Scita, G., and Di Fiore, P. P. (2012) Endocytosis and signaling: cell logistics shape the eukaryotic cell plan. *Physiol. Rev.* **92,** 273–366
2. McMahon, H. T., and Boucrot, E. (2011) Molecular mechanism and physiological functions of clathrin-mediated endocytosis. *Nat. Rev. Mol. Cell Biol.* **12,** 517–533
3. Mayor, S., and Pagano, R. E. (2007) Pathways of clathrin-independent endocytosis. *Nat. Rev. Mol. Cell Biol.* **8,** 603–612
4. Breslow, D. K., and Weissman, J. S. (2010) Membranes in balance: mechanisms of sphingolipid homeostasis. *Mol. Cell.* **40,** 267–279
5. Hannich, J. T., Umebayashi, K., and Riezman, H. (2011) Distribution and functions of sterols and sphingolipids. *Cold Spring Harb. Perspect. Biol.* **3,** a004762
6. Morgan, J., McCourt, P., Rankin, L., Swain, E., Rice, L. M., and Nickels, J. T., Jr. (2009) Altering sphingolipid metabolism in *Saccharomyces cerevisiae* cells lacking the amphiphysin ortholog Rvs161 reinitiates sugar transporter endocytosis. *Eukaryot. Cell* **8,** 779–789
7. Youn, J. Y., Friesen, H., Kishimoto, T., Henne, W. M., Kurat, C. F., Ye, W., Ceccarelli, D. F., Sicheri, F., Kohlwein, S. D., McMahon, H. T., and Andrews, B. J. (2010) Dissecting BAR domain function in the yeast Amphiphysins Rvs161 and Rvs167 during endocytosis. *Mol. Biol. Cell* **21,** 3054–3069
8. Kjaerulff, O., Brodin, L., and Jung, A. (2011) The structure and function of endophilin proteins. *Cell Biochem. Biophys.* **60,** 137–154
9. Aguilar, P. S., Fröhlich, F., Rehman, M., Shales, M., Ulitsky, I., Olivera-Couto, A., Braberg, H., Shamir, R., Walter, P., Mann, M., Ejsing, C. S., Krogan, N. J., and Walther, T. C. (2010) A plasma-membrane E-MAP reveals links of the eisosome with sphingolipid metabolism and endosomal trafficking. *Nat. Struct. Mol. Biol.* **17,** 901–908
10. Yonamine, I., Bamba, T., Nirala, N. K., Jesmin, N., Kosakowska-Cholody, T., Nagashima, K., Fukusaki, E., Acharya, J. K., and Acharya, U. (2011) Sphingosine kinases and their metabolites modulate endolysosomal trafficking in photoreceptors. *J. Cell Biol.* **192,** 557–567
11. Chan, J. P., Hu, Z., and Sieburth, D. (2012) Recruitment of sphingosine kinase to presynaptic terminals by a conserved muscarinic signaling pathway promotes neurotransmitter release. *Genes Dev.* **26,** 1070–1085
12. Chan, J. P., and Sieburth, D. (2012) Localized sphingolipid signaling at presynaptic terminals is regulated by calcium influx and promotes recruitment of priming factors. *J. Neurosci.* **32,** 17909–17920
13. Hayashi, S., Okada, T., Igarashi, N., Fujita, T., Jahangeer, S., and Nakamura, S. (2002) Identification and characterization of RPK118, a novel sphingosine kinase-1-binding protein. *J. Biol. Chem.* **277,** 33319–33324
14. Thompson, C. R., Iyer, S. S., Melrose, N., VanOosten, R., Johnson, K., Pitson, S. M., Obeid, L. M., and Kusner, D. J. (2005) Sphingosine kinase 1 (SK1) is recruited to nascent phagosomes in human macrophages: inhibition of SK1 translocation by *Mycobacterium tuberculosis*. *J. Immunol.* **174,** 3551–3561
15. Kusner, D. J., Thompson, C. R., Melrose, N. A., Pitson, S. M., Obeid, L. M., and Iyer, S. S. (2007) The localization and activity of sphingosine kinase 1 are coordinately regulated with actin cytoskeletal dynamics in macrophages. *J. Biol. Chem.* **282,** 23147–23162
16. Shen, H., Giordano, F., Wu, Y., Chan, J., Zhu, C., Milosevic, I., Wu, X., Yao, K., Chen, B., Baumgart, T., Sieburth, D., and De Camilli, P. (2014) Coupling between endocytosis and sphingosine kinase 1 recruitment. *Nat. Cell Biol.* **16,** 652–662
17. Paugh, S. W., Paugh, B. S., Rahmani, M., Kapitonov, D., Almenara, J. A., Kordula, T., Milstien, S., Adams, J. K., Zipkin, R. E., Grant, S., and Spiegel, S. (2008) A selective sphingosine kinase 1 inhibitor integrates multiple molecular therapeutic targets in human leukemia. *Blood* **112,** 1382–1391
18. Schnute, M. E., McReynolds, M. D., Kasten, T., Yates, M., Jerome, G., Rains, J. W., Hall, T., Chrencik, J., Kraus, M., Cronin, C. N., Saabye, M., Highkin, M. K., Broadus, R., Ogawa, S., Cukyne, K., *et al.* (2012) Modulation of cellular S1P levels with a novel, potent and specific inhibitor of sphingosine kinase-1. *Biochem. J.* **444,** 79–88
19. Brinkmann, V., Billich, A., Baumruker, T., Heining, P., Schmouder, R., Francis, G., Aradhye, S., and Burtin, P. (2010) Fingolimod (FTY720): discovery and development of an oral drug to treat multiple sclerosis. *Nat. Rev. Drug Discov.* **9,** 883–897
20. Paugh, S. W., Payne, S. G., Barbour, S. E., Milstien, S., and Spiegel, S. (2003) The immunosuppressant FTY720 is phosphorylated by sphingosine kinase type 2. *FEBS Lett.* **554,** 189–193
21. Romero Rosales, K., Singh, G., Wu, K., Chen, J., Janes, M. R., Lilly, M. B., Peralta, E. R., Siskind, L. J., Bennett, M. J., Fruman, D. A., and Edinger, A. L. (2011) Sphingolipid-based drugs selectively kill cancer cells by down-regulating nutrient transporter proteins. *Biochem. J.* **439,** 299–311

22. Li, L., Wan, T., Wan, M., Liu, B., Cheng, R., and Zhang, R. (2015) The effect of the size of fluorescent dextran on its endocytic pathway. *Cell Biol. Int.* **39,** 531–539
23. Villamil Giraldo, A. M., Appelqvist, H., Ederth, T., and Öllinger, K. (2014) Lysosomotropic agents: impact on lysosomal membrane permeabilization and cell death. *Biochem. Soc. Trans.* **42,** 1460–1464
24. Shichiri, M., Kono, N., Shimanaka, Y., Tanito, M., Rotzoll, D. E., Yoshida, Y., Hagihara, Y., Tamai, H., and Arai, H. (2012) A novel role for α-tocopherol transfer protein (α-TTP) in protecting against chloroquine toxicity. *J. Biol. Chem.* **287,** 2926–2934
25. Michihara, A., Toda, K., Kubo, T., Fujiwara, Y., Akasaki, K., and Tsuji, H. (2005) Disruptive effect of chloroquine on lysosomes in cultured rat hepatocytes. *Biol. Pharm. Bull.* **28,** 947–951
26. Puchkov, D., and Haucke, V. (2013) Greasing the synaptic vesicle cycle by membrane lipids. *Trends Cell Biol.* **23,** 493–503
27. Rodal, S. K., Skretting, G., Garred, O., Vilhardt, F., van Deurs, B., and Sandvig, K. (1999) Extraction of cholesterol with methyl-β-cyclodextrin perturbs formation of clathrin-coated endocytic vesicles. *Mol. Biol. Cell* **10,** 961–974
28. Subtil, A., Gaidarov, I., Kobylarz, K., Lampson, M. A., Keen, J. H., and McGraw, T. E. (1999) Acute cholesterol depletion inhibits clathrin-coated pit budding. *Proc. Natl. Acad. Sci. U.S.A.* **96,** 6775–6780
29. Höglinger, D., Haberkant, P., Aguilera-Romero, A., Riezman, H., Porter, F. D., Platt, F. M., Galione, A., and Schultz, C. (2015) Intracellular sphingosine releases calcium from lysosomes. *eLife* **4,** e10616
30. Stenmark, H. (2009) Rab GTPases as coordinators of vesicle traffic. *Nat. Rev. Mol. Cell Biol.* **10,** 513–525
31. Tooze, S. A., Abada, A., and Elazar, Z. (2014) Endocytosis and autophagy: exploitation or cooperation? *Cold Spring Harb. Perspect. Biol.* **6,** a018358
32. Hyttinen, J. M., Niittykoski, M., Salminen, A., and Kaarniranta, K. (2013) Maturation of autophagosomes and endosomes: a key role for Rab7. *Biochim. Biophys. Acta* **1833,** 503–510
33. Huotari, J., and Helenius, A. (2011) Endosome maturation. *EMBO J.* **30,** 3481–3500
34. Ivanov, A. I. (2008) Pharmacological inhibition of endocytic pathways: is it specific enough to be useful? *Methods Mol. Biol.* **440,** 15–33
35. Dutta, D., and Donaldson, J. G. (2012) Search for inhibitors of endocytosis: intended specificity and unintended consequences. *Cell Logist.* **2,** 203–208
36. Yoshimori, T., Yamamoto, A., Moriyama, Y., Futai, M., and Tashiro, Y. (1991) Bafilomycin A1, a specific inhibitor of vacuolar-type H^+-ATPase, inhibits acidification and protein degradation in lysosomes of cultured cells. *J. Biol. Chem.* **266,** 17707–17712
37. Boucrot, E., Ferreira, A. P., Almeida-Souza, L., Debard, S., Vallis, Y., Howard, G., Bertot, L., Sauvonnet, N., and McMahon, H. T. (2015) Endophilin marks and controls a clathrin-independent endocytic pathway. *Nature* **517,** 460–465
38. Ramstedt, B., and Slotte, J. P. (2006) Sphingolipids and the formation of sterol-enriched ordered membrane domains. *Biochim. Biophys. Acta* **1758,** 1945–1956
39. Brown, D. A., and London, E. (2000) Structure and function of sphingolipid- and cholesterol-rich membrane rafts. *J. Biol. Chem.* **275,** 17221–17224
40. Torgersen, M. L., Skretting, G., van Deurs, B., and Sandvig, K. (2001) Internalization of cholera toxin by different endocytic mechanisms. *J. Cell Sci.* **114,** 3737–3747
41. Renard, H. F., Simunovic, M., Lemière, J., Boucrot, E., Garcia-Castillo, M. D., Arumugam, S., Chambon, V., Lamaze, C., Wunder, C., Kenworthy, A. K., Schmidt, A. A., McMahon, H. T., Sykes, C., Bassereau, P., and Johannes, L. (2015) Endophilin-A2 functions in membrane scission in clathrin-independent endocytosis. *Nature* **517,** 493–496
42. Jarsch, I. K., Daste, F., and Gallop, J. L. (2016) Membrane curvature in cell biology: an integration of molecular mechanisms. *J. Cell Biol.* **214,** 375–387
43. Takahashi, Y., Meyerkord, C. L., and Wang, H. G. (2009) Bif-1/endophilin B1: a candidate for crescent driving force in autophagy. *Cell Death Differ.* **16,** 947–955
44. Young, M. M., Takahashi, Y., Fox, T. E., Yun, J. K., Kester, M., and Wang, H. G. (2016) Sphingosine kinase 1 cooperates with autophagy to maintain endocytic membrane trafficking. *Cell Rep.* **17,** 1532–1545
45. Lee, H., Lee, J. K., Park, M. H., Hong, Y. R., Marti, H. H., Kim, H., Okada, Y., Otsu, M., Seo, E. J., Park, J. H., Bae, J. H., Okino, N., He, X., Schuchman, E. H., Bae, J. S., and Jin, H. K. (2014) Pathological roles of the VEGF/SphK pathway in Niemann-Pick type C neurons. *Nat. Commun.* **5,** 5514
46. Mora, R., Dokic, I., Kees, T., Hüber, C. M., Keitel, D., Geibig, R., Brügge, B., Zentgraf, H., Brady, N. R., and Régnier-Vigouroux, A. (2010) Sphingolipid rheostat alterations related to transformation can be exploited for specific induction of lysosomal cell death in murine and human glioma. *Glia* **58,** 1364–1383
47. Lloyd-Evans, E., Morgan, A. J., He, X., Smith, D. A., Elliot-Smith, E., Sillence, D. J., Churchill, G. C., Schuchman, E. H., Galione, A., and Platt, F. M. (2008) Niemann-Pick disease type C1 is a sphingosine storage disease that causes deregulation of lysosomal calcium. *Nat. Med.* **14,** 1247–1255
48. Collinet, C., Stöter, M., Bradshaw, C. R., Samusik, N., Rink, J. C., Kenski, D., Habermann, B., Buchholz, F., Henschel, R., Mueller, M. S., Nagel, W. E., Fava, E., Kalaidzidis, Y., and Zerial, M. (2010) Systems survey of endocytosis by multiparametric image analysis. *Nature* **464,** 243–249
49. Mizugishi, K., Yamashita, T., Olivera, A., Miller, G. F., Spiegel, S., and Proia, R. L. (2005) Essential role for sphingosine kinases in neural and vascular development. *Mol. Cell. Biol.* **25,** 11113–11121
50. D'Hondt, K., Heese-Peck, A., and Riezman, H. (2000) Protein and lipid requirements for endocytosis. *Annu. Rev. Genet.* **34,** 255–295
51. Dickson, R. C. (2008) Thematic review series: sphingolipids: new insights into sphingolipid metabolism and function in budding yeast. *J. Lipid Res.* **49,** 909–921
52. Zanolari, B., Friant, S., Funato, K., Sütterlin, C., Stevenson, B. J., and Riezman, H. (2000) Sphingoid base synthesis requirement for endocytosis in *Saccharomyces cerevisiae*. *EMBO J.* **19,** 2824–2833
53. Friant, S., Zanolari, B., and Riezman, H. (2000) Increased protein kinase or decreased PP2A activity bypasses sphingoid base requirement in endocytosis. *EMBO J.* **19,** 2834–2844
54. Liu, K., Zhang, X., Lester, R. L., and Dickson, R. C. (2005) The sphingoid long chain base phytosphingosine activates AGC-type protein kinases in *Saccharomyces cerevisiae*, including Ypk1, Ypk2, and Sch9. *J. Biol. Chem.* **280,** 22679–22687
55. deHart, A. K., Schnell, J. D., Allen, D. A., and Hicke, L. (2002) The conserved Pkh-Ypk kinase cascade is required for endocytosis in yeast. *J. Cell Biol.* **156,** 241–248
56. Meyer, S. G., Wendt, A. E., Scherer, M., Liebisch, G., Kerkweg, U., Schmitz, G., and de Groot, H. (2012) Myriocin, an inhibitor of serine palmitoyl transferase, impairs the uptake of transferrin and low-density lipoprotein in mammalian cells. *Arch. Biochem. Biophys.* **526,** 60–68
57. Goñi, F. M., Sot, J., and Alonso, A. (2014) Biophysical properties of sphingosine, ceramides and other simple sphingolipids. *Biochem. Soc. Trans.* **42,** 1401–1408
58. Contreras, F. X., Sot, J., Alonso, A., and Goñi, F. M. (2006) Sphingosine increases the permeability of model and cell membranes. *Biophys. J.* **90,** 4085–4092
59. Georgieva, R., Koumanov, K., Momchilova, A., Tessier, C., and Staneva, G. (2010) Effect of sphingosine on domain morphology in giant vesicles. *J. Colloid Interface Sci.* **350,** 502–510
60. Milosevic, I., Giovedi, S., Lou, X., Raimondi, A., Collesi, C., Shen, H., Paradise, S., O'Toole, E., Ferguson, S., Cremona, O., and De Camilli, P. (2011) Recruitment of endophilin to clathrin-coated pit necks is required for efficient vesicle uncoating after fission. *Neuron* **72,** 587–601
61. Ferguson, S. M., Ferguson, S., Raimondi, A., Paradise, S., Shen, H., Mesaki, K., Ferguson, A., Destaing, O., Ko, G., Takasaki, J., Cremona, O., O'Toole, E., and De Camilli, P. (2009) Coordinated actions of actin and BAR proteins upstream of dynamin at endocytic clathrin-coated pits. *Dev. Cell* **17,** 811–822
62. Ringstad, N., Gad, H., Löw, P., Di Paolo, G., Brodin, L., Shupliakov, O., and De Camilli, P. (1999) Endophilin/SH3p4 is required for the transition from early to late stages in clathrin-mediated synaptic vesicle endocytosis. *Neuron* **24,** 143–154

63. Cuddeback, S. M., Yamaguchi, H., Komatsu, K., Miyashita, T., Yamada, M., Wu, C., Singh, S., and Wang, H. G. (2001) Molecular cloning and characterization of Bif-1. A novel Src homology 3 domain-containing protein that associates with Bax. *J. Biol. Chem.* **276,** 20559–20565
64. Karbowski, M., Jeong, S. Y., and Youle, R. J. (2004) Endophilin B1 is required for the maintenance of mitochondrial morphology. *J. Cell Biol.* **166,** 1027–1039
65. Takahashi, Y., Coppola, D., Matsushita, N., Cualing, H. D., Sun, M., Sato, Y., Liang, C., Jung, J. U., Cheng, J. Q., Mulé, J. J., Pledger, W. J., and Wang, H. G. (2007) Bif-1 interacts with Beclin 1 through UVRAG and regulates autophagy and tumorigenesis. *Nat. Cell Biol.* **9,** 1142–1151
66. Boulakirba, S., Macia, E., Partisani, M., Lacas-Gervais, S., Brau, F., Luton, F., and Franco, M. (2014) Arf6 exchange factor EFA6 and endophilin directly interact at the plasma membrane to control clathrin-mediated endocytosis. *Proc. Natl. Acad. Sci. U.S.A.* **111,** 9473–9478
67. Runkle, K. B., Meyerkord, C. L., Desai, N. V., Takahashi, Y., and Wang, H. G. (2012) Bif-1 suppresses breast cancer cell migration by promoting EGFR endocytic degradation. *Cancer Biol. Ther.* **13,** 956–966
68. Liang, C., Lee, J. S., Inn, K. S., Gack, M. U., Li, Q., Roberts, E. A., Vergne, I., Deretic, V., Feng, P., Akazawa, C., and Jung, J. U. (2008) Beclin1-binding UVRAG targets the class C Vps complex to coordinate autophagosome maturation and endocytic trafficking. *Nat. Cell Biol.* **10,** 776–787
69. Thoresen, S. B., Pedersen, N. M., Liestøl, K., and Stenmark, H. (2010) A phosphatidylinositol 3-kinase class III sub-complex containing VPS15, VPS34, Beclin 1, UVRAG and BIF-1 regulates cytokinesis and degradative endocytic traffic. *Exp. Cell Res.* **316,** 3368–3378
70. Mellman, I., and Yarden, Y. (2013) Endocytosis and cancer. *Cold Spring Harb. Perspect. Biol.* **5,** a016949
71. Platt, F. M. (2014) Sphingolipid lysosomal storage disorders. *Nature* **510,** 68–75
72. Maxfield, F. R. (2014) Role of endosomes and lysosomes in human disease. *Cold Spring Harb. Perspect. Biol.* **6,** a016931
73. Maceyka, M., Alvarez, S. E., Milstien, S., and Spiegel, S. (2008) Filamin A links sphingosine kinase 1 and sphingosine-1-phosphate receptor 1 at lamellipodia to orchestrate cell migration. *Mol. Cell Biol.* **28,** 5687–5697
74. Olivera, A., Kohama, T., Edsall, L., Nava, V., Cuvillier, O., Poulton, S., and Spiegel, S. (1999) Sphingosine kinase expression increases intracellular sphingosine-1-phosphate and promotes cell growth and survival. *J. Cell Biol.* **147,** 545–558
75. Schneider, C. A., Rasband, W. S., and Eliceiri, K. W. (2012) NIH Image to ImageJ: 25 years of image analysis. *Nat. Methods* **9,** 671–675
76. Lima, S., Milstien, S., and Spiegel, S. (2014) A real-time high-throughput fluorescence assay for sphingosine kinases. *J. Lipid Res.* **55,** 1525–1530